



ELSEVIER

Available online at www.sciencedirect.com



International Journal of Solids and Structures 43 (2006) 5994–6013

INTERNATIONAL JOURNAL OF
**SOLIDS and
STRUCTURES**

www.elsevier.com/locate/ijssolstr

The plastic zone size in indentation experiments: The analogy with the expansion of a spherical cavity

M. Mata, O. Casals, J. Alcalá *

Department of Materials Science and Metallurgical Engineering, E.T.S.E.I.B., Universitat Politècnica de Catalunya, Barcelona 08028, Spain

Received 19 May 2005

Available online 9 September 2005

Abstract

This paper provides in-depth examinations of the well-known analogy between indentation experiments and the expansion of a spherical cavity. Closed-form solutions are derived for the extension of the plastic zone in perfectly plastic and strain hardening solids. The theoretical analysis takes into account the role of elastic and plastic deformations in the overall contact response, leading to accurate solutions for cavity inflation. Presently proposed analogy is based on comprehensive finite element simulations of conical, spherical and pyramidal indentation, which allow us to find a correspondence between the parameters describing the contact response and those in expanding cavity formulations. Such parametrical identification has the advantage to hold true both in expanding cavity formulations for perfectly plastic solids and in those derived herein for strain hardening solids. Attention is given to the assessment of the plastic zone along the indented surface, as well as to quantify the influence of further plastic flow induced upon load removal on the plastic zone size.

© 2005 Elsevier Ltd. All rights reserved.

Keywords: Indentation; Contact mechanics; Plasticity; Finite element simulations; Hardness

1. Introduction

A characteristic feature of indentation experiments is the development of a plastic zone, whose size increases during load application. Among other aspects, knowledge of the plastic zone size allows: (i) extraction of yield strength; (ii) examination, within a continuum mechanics framework, of discrete deformation processes occurring at small loads; and (iii) assessment of the possible influence of the substrate on the contact response of thin films and small-volume structures (see [Li and Bradt, 1993](#); [Yoshioka, 1994](#); [Kramer](#)

* Corresponding author. Tel.: +34 93 4016287; fax: +34 93 4016706.

E-mail address: jorge.alcala@upc.es (J. Alcalá).

et al., 1999; Elmustafa et al., 2000; Huang et al., 2000; Puech et al., 2000; Woodcock and Bahr, 2000; Chiu and Ngan, 2002; Elmustafa and Stone, 2002). In addition, the shape of the plastic zone is indicative of the plastic flow features underneath the indenter. It is known that elasticity plays a fundamental role in indentation experiments when the plastic zone is confined underneath the indenter's tip. On the other hand, elastic strains play a secondary effect within the fully plastic contact regime, where the plastic zone spreads outwards from the indenter (Johnson, 1985; Mata et al., 2002).

Mechanistic interpretations to indentation experiments have long been based on the analogy between indentation and the expansion of a spherical cavity (Bishop et al., 1945; Johnson, 1970; Chiang et al., 1982). This analogy provides useful relationships between contact parameters, such as hardness and plastic zone size, and the elasto-plastic mechanical properties of the material. In particular, Johnson's model allows one to predict the plastic zone size c from

$$\left(\frac{c}{a_s}\right)^3 = \frac{1}{3 \tan \theta} \frac{E}{\sigma_{ys}}, \quad (1)$$

where a_s is the radius of the imprint (which is equivalent to the radius of the spherical cavity), E is the Young's modulus, σ_{ys} is the yield strength, and θ is the semi-apical angle of the conical indenter. Although this equation has been employed in the analysis of indentation experiments (see, for instance, Johnson, 1970; Li and Bradt, 1993; Yoshioka, 1994; Kramer et al., 1999; Elmustafa et al., 2000; Huang et al., 2000; Puech et al., 2000; Woodcock and Bahr, 2000; Chiu and Ngan, 2002; Elmustafa and Stone, 2002), the underlying analogy between indentation parameters and those ruling the expansion of the cavity has not been thoroughly examined. Furthermore, the above indentation models require definition of a hydrostatic core to act as the inflating spherical cavity (Johnson, 1970; Chiang et al., 1982). The physical rationale behind the conception of the core remains rather obscure, as it comprises both the rigid indenter and the surrounding material within a single concept. Also, the hydrostatic nature of the core is controversial in light of the large shear stresses and extensive plastic flow attained directly underneath the indenter.

An important limitation in Eq. (1) is that it ignores strain hardening effects, as it is derived for elastic-perfectly plastic solids. Formulations to incorporate strain hardening into the analysis of the expanding cavity were given by Chadwick (1959), Durban and Baruch (1976), Chiang et al. (1982), Bignoni and Ludiero (1989) and Lubliner (1990). These investigations focused on the internal pressure at the cavity which, according to Johnson's model, is linearly related to hardness. Although such analyses on strain-hardening solids succeeded in finding integral-form relations for the internal pressure as a function of the plastic zone size, attempts were not made at deriving closed-form relations between the plastic zone and the mechanical properties of the solid.

The main purpose of this paper is to review the analogy between indentation and the expansion of a cavity. Present analogy is laid upon the closed-form solutions for cavity inflation in perfectly plastic and strain hardening solids derived in the paper, as well as on a strict equivalency between the variables in these formulations and those describing indentation experiments. This paper is arranged in the following sections. First, formulations for the internal pressure leading to cavity inflation in elastic-power-law plastic solids are derived in Section 2. These equations, in conjunction with extensive finite element simulations of spherical and conical indentation, are used in Sections 4 and 5 to establish the parametrical analogy between indentation and the expansion of the cavity. The present analysis leads to closed-form solutions for the prediction of plastic zone size in indentation experiments in terms of uniaxial properties and hardness values. Three-dimensional finite element simulations of pyramidal indentation are finally used in Section 6 to address the issue of how to extend the present framework to Vickers and Berkovich indentation experiments, as well as to evaluate the influence of load removal upon the extension of the plastic zone.

2. The expansion of a spherical cavity in an infinite medium

2.1. General framework

In this section, an overview is given on the existing formulations describing inflation of a spherical cavity (Hill, 1950; Lubliner, 1990). Fig. 1 illustrates a cavity of instantaneous radius R_i which expands radially into an infinite space. Inflation of the cavity exerts hydrostatic pressure at the surface which modifies the stress–strain state of the surrounding medium.

Upon an early elastic behavior of the solid, further inflation leads to the onset of plastic deformation at a critical value of internal pressure p_{cav} . An elastic–plastic boundary of radius c is thus induced, where for $\rho > c$ the solid remains elastic, Fig. 1. Owing to spherical symmetry, stresses and strains are expressed in terms of radial position ρ . By virtue of spherical symmetry, the stress state is taken as the sum of a fully hydrostatic state $(\sigma_\theta, \sigma_\theta, \sigma_\theta)$ and compressive state $(\sigma_\rho - \sigma_\theta, 0, 0)$; see Hill (1950). Hence, the von Mises yield condition implies that

$$\sigma_\theta - \sigma_\rho = Y(\epsilon), \quad (2)$$

where $Y(\epsilon)$ is the uniaxial strain-hardening law of the solid, which is taken to obey

$$\sigma = \begin{cases} E\epsilon & \text{if } \epsilon \leq \epsilon_{ys}, \\ Y(\epsilon) = \sigma_0 \epsilon^n & \text{otherwise.} \end{cases} \quad (3)$$

In Eq. (3), ϵ is the sum of the elastic and plastic uniaxial strains ($\epsilon = \epsilon_{el} + \epsilon_{pl}$), E is the Young's modulus, and n is the power-law strain-hardening coefficient. For continuity of the stress–strain relation at $\epsilon = \epsilon_{ys}$, it necessarily follows that $\sigma_0 = \sigma_{ys}^{1-n} E^n$.

As the stresses are continuous across the elastic–plastic boundary, the internal pressure p_{cav} leading to plastic flow is (Hill, 1950; Lubliner, 1990)

$$p_{cav} = \frac{2}{3} \sigma_{ys} + 2 \int_R^c Y(\epsilon) \frac{d\rho}{\rho}. \quad (4)$$

Attention is now drawn to describe cavity growth in terms of the plastic zone size and the mechanical properties of the solid. Treating the elastic–plastic boundary as elastic and compressible, relative plastic zone size c/R is given by (Hill, 1950)

$$\frac{dR}{dc} = \frac{3(1-\nu)Y(\epsilon)c^2}{ER^2} - \frac{2(1-2\nu)Y(\epsilon)R}{Ec}. \quad (5)$$

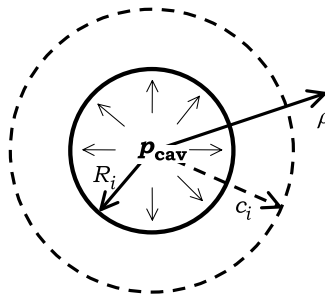


Fig. 1. Expansion of a spherical cavity of instantaneous radius R_i and plastic zone c_i induced by hydrostatic pressure p_{cav} . ρ is the radial coordinate.

For simplicity in solving Eq. (5), plastic incompressibility is assumed for $\rho < c$ (i.e., Poisson's ratio, $\nu = 0.5$). This is a sensible approximation as ν has little influence on plastic zone size c (Chadwick, 1959). The second term in the right-hand side of Eq. (5) thus vanishes, leading to a separate-variable differential equation. Integration yields

$$R^3 - R_0^3 = \frac{3}{2E} \int_{c_0}^c 3\rho^2 Y(\epsilon) d\rho, \quad (6)$$

where R_0 is the cavity radius corresponding to plastic zone c_0 . In contrast to Eq. (4), which describes an instantaneous state in the inflation of the cavity, Eq. (6) concerns its *evolution* from initial conditions R_0 and c_0 . Finding closed-form solutions for Eq. (6) thus requires prior knowledge of variables R_0 and c_0 .

A particular case in the above analyses pertains to elastic–*perfectly* plastic solids, $n = 0$ and $Y(\epsilon) = \sigma_{ys}$ (Hill, 1950). Integration of Eq. (4) leads to

$$p_{cav} = \frac{2}{3} \sigma_{ys} \left[1 + 3 \ln \left(\frac{c}{R} \right) \right]. \quad (7)$$

In addition, the well-known relation for the relative plastic zone size is obtained from Eq. (6):

$$\frac{c}{R} = \left(\frac{2E}{3\sigma_{ys}} \right)^{1/3}, \quad (8)$$

where it is assumed that $R_0 = c_0 = 0$ (Hill, 1950). Alternatively, considering that linear elasticity still applies at the elastic–plastic boundary ($\rho = c$), substitution of elastic solutions for σ_θ and σ_ρ into Eq. (2) also allows derivation of Eq. (8) (Hill, 1950; Lubliner, 1990).

2.2. Fully plastic response

Integration of Eq. (4) is performed herein neglecting the influence of elastic strains within the plastic zone (i.e., $\epsilon = \epsilon_{pl}$). The analysis pertains to the inflation of a cavity in solids whose local strains within the plastic zone are dominated by plastic flow, while elastic deformation is allowed to occur in the surrounding media. The applicability of such an approximation to indentation experiments of solids exhibiting various degrees of elasto-plastic deformation is examined in Section 5.2.

Since the displacements are radial, plastic incompressibility allows one to find the following equation for the radial deformation within the plastic zone (Hill, 1950; Lubliner, 1990):

$$\epsilon_{pl} = 2 \ln \left(\frac{\rho}{\rho_0} \right) = \frac{2}{3} \ln \left(\frac{\rho^3}{\rho_0^3 - R^3} \right). \quad (9)$$

Eq. (9) prescribes the instantaneous deformation of a generic material-point at distance ρ with respect to its initial position ρ_0 (ρ and ρ_0 are within plastic zones c and c_0 , respectively). In deriving Eq. (9), it is further assumed that $R_0 = 0$.

Again, taking $\epsilon = \epsilon_{pl}$, substitution of Eq. (9) into Eq. (3) implies that

$$Y(\epsilon) = \sigma_0 \left(\frac{2}{3} \ln \left(\frac{\rho^3}{\rho_0^3 - R^3} \right) \right)^n. \quad (10)$$

Further substitution of Eq. (10) into Eq. (4) yields

$$p_{cav} = \frac{2}{3} \sigma_{ys} + 2 \int_R^c \sigma_0 \left(\frac{2}{3} \ln \left(\frac{\rho^3}{\rho_0^3 - R^3} \right) \right)^n \frac{d\rho}{\rho}. \quad (11)$$

By taking $t = \rho/R$, Eq. (11) transforms to

$$p_{\text{cav}} = \frac{2}{3}\sigma_{\text{ys}} + 2\sigma_0 \int_1^{c/R} \left(\frac{2}{3} \ln \left(\frac{t^3}{t^3-1} \right) \right)^n \frac{dt}{t}. \quad (12)$$

Eq. (12) provides a fundamental relationship between cavity pressure p_{cav} ; mechanical properties σ_{ys} , σ_0 and n ; and relative plastic zone size c/R . However, to our knowledge, the integral in Eq. (12) lacks of analytical solution. The approach adopted herein to solve Eq. (12) is thus to replace the integrand with a simple integrable best-fit function. It is remarked that although the integrand diverges for $t = 1$, the integral in Eq. (12) is necessarily finite as σ_{ys} and p_{cav} are bounded quantities.

Hence, we seek to find $f(t, n)$ so that

$$f(t, n) = A(n)t^{B(n)} \simeq \left(\frac{2}{3} \ln \left(\frac{t^3}{t^3-1} \right) \right)^n \frac{1}{t} \quad \text{for } t \geq x(n), \quad (13)$$

where $x(n)$ is the value of t below which $f(t, n)$ starts to depart from the integrand, Fig. 2. Functional analysis is then used to obtain constants A and B best-fitting Eq. (13) for discrete values of strain-hardening coefficient n . Representation of $f = A(n)t^{B(n)}$ readily confirms that for optimum values of A and B , this simple functional form adjusts extremely well to the integrand (provided $t \geq x(n)$), Fig. 2. To solve the integral, we impose

$$2\sigma_0 \int_1^{c/R} \left(\frac{2}{3} \ln \left(\frac{t^3}{t^3-1} \right) \right)^n \frac{dt}{t} = 2\sigma_0 N_0(n) + 2\sigma_0 \int_{x(n)}^{c/R} f(t, n) dt, \quad (14)$$

where $2\sigma_0 N_0(n)$ estimates the diverging part of the integral from $t = 1$ to $t = x(n)$. The actual value of $N_0(n)$ is then obtained through a numerical integration scheme.

Finally, substituting Eq. (14) into Eq. (12),

$$\frac{p_{\text{cav}}}{\sigma_0} = \frac{2}{3} \frac{\sigma_{\text{ys}}}{\sigma_0} + 2N_0(n) + 2M_0(n) \left[\left(\frac{c}{R} \right)^{P(n)} - x(n)^{P(n)} \right], \quad (15)$$

where

$$M_0(n) = \frac{A(n)}{B(n)+1} \quad \text{and} \quad P(n) = B(n) + 1.$$

We now direct attention to the early work by Tabor, where hardness H is normalized with respect to a representative uniaxial stress σ_r (Tabor, 1951). Since hardness H is related to p_{cav} in the expanding cavity

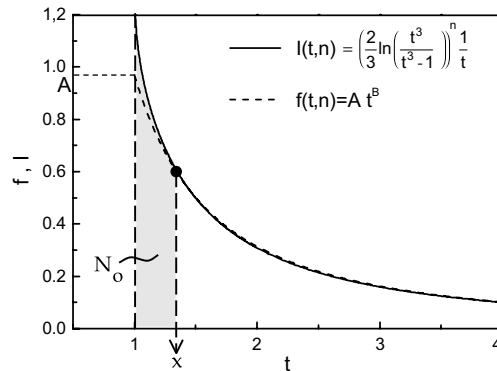


Fig. 2. Comparison between integrand I in Eq. (12) and approximative function $f(t) = At^B$ for $n = 0.2$.

analogy, it is pertinent to recast Eq. (15) using ratio p_{cav}/σ_r rather than p_{cav}/σ_0 . In the spirit of Tabor's work, stress level σ_r is defined at a uniaxial material-independent representative deformation $\epsilon_r = 0.1$, so that H/σ_r happens to be 2.7 in all solids whose contact response is plastically dominated (Tabor, 1951; Atkins and Tabor, 1965; Dao et al., 2001; Larsson, 2001; Mata et al., 2002; Xu and Rowcliffe, 2002). From the uniaxial stress–strain relation (Eq. (3)), it follows that

$$\sigma_r = \sigma_{\text{ys}}^{1-n} (0.1E)^n. \quad (16)$$

Thus, replacing variable σ_0 for σ_r in Eq. (15)

$$\frac{p_{\text{cav}}}{\sigma_r} = \frac{2}{3} \left(\frac{\epsilon_{\text{ys}}}{\epsilon_r} \right)^n + \Theta(n) + M(n) \left(\frac{c}{R} \right)^{P(n)}, \quad (17)$$

where

$$\Theta(n) = N(n) - M(n)x(n)^{P(n)}, \quad N(n) = \frac{2N_0(n)}{\epsilon_r^n} \quad \text{and} \quad M(n) = \frac{2M_0(n)}{\epsilon_r^n}.$$

The functions listed below are then found through the best-fit values of $A(n)$ and $B(n)$ for each $x(n)$

$$\Theta(n) = 2.5968 + \frac{0.5097}{n}, \quad (18)$$

$$M(n) = -2.2778 - \frac{0.5479}{n}, \quad (19)$$

$$P(n) = -3.0615n - 0.005. \quad (20)$$

2.3. Elasto-plastic response

In this section, we aim at extending the above analysis for fully plastic solids to account for the influence of elastic strains within the plastic zone. We thus seek to derive an integral equation for p_{cav}/σ_0 that explicitly incorporates the role of elastic strains. As described in Section 5.2, this analysis is relevant to indentation experiments in solids whose contact response is significantly affected by elasticity (that is to say, those deforming within the elasto-plastic contact regime (Mata et al., 2002)).

Following Eq. (3), the uniaxial strain-hardening law of the solid is assumed to obey

$$Y(\epsilon) = \sigma_0(\epsilon_{\text{pl}} + \epsilon_{\text{el}})^n = \sigma_0 \left(\epsilon_{\text{pl}} + \frac{\sigma}{E} \right)^n. \quad (21)$$

Performing a Taylor's series expansion for elastic strains smaller than plastic strains, we write

$$\left(\epsilon_{\text{pl}} + \frac{\sigma}{E} \right)^n \simeq \epsilon_{\text{pl}}^n \left(1 + n \frac{\sigma/E}{\epsilon_{\text{pl}}} \right). \quad (22)$$

Hence,

$$Y(\epsilon) \simeq \sigma_0 \left(\epsilon_{\text{pl}}^n + n \epsilon_{\text{pl}}^{n-1} \frac{\sigma}{E} \right) \simeq \sigma_0 \epsilon_{\text{pl}}^n + \frac{\sigma_0^2}{E} n \epsilon_{\text{pl}}^{2n-1}, \quad (23)$$

where $n \frac{\sigma/E}{\epsilon_{\text{pl}}}$ has been neglected in further expansions.

The same analysis as in the previous sections is then conducted by substituting the approximative stress–strain relation in Eq. (23) into Eq. (4). After some rearrangements, we find

$$p_{\text{cav}} = \frac{2}{3} \sigma_{\text{ys}} + 2\sigma_0 \int_1^{c/R} \left(\frac{2}{3} \ln \left(\frac{t^3}{t^3 - 1} \right) \right)^n \frac{dt}{t} + 2n \frac{\sigma_0^2}{E} \int_1^{c/R} \left(\frac{2}{3} \ln \left(\frac{t^3}{t^3 - 1} \right) \right)^{2n-1} \frac{dt}{t}. \quad (24)$$

By virtue of the approximation made in Eq. (23), note that the right-hand side of Eq. (24) is composed by three terms. A relevant feature in this formulation is that, comparing Eq. (24) with Eq. (12), one can readily see that as the first two terms correspond to the fully plastic solution, the influence of elastic strains is necessarily captured through the third term. The second term dominates over the third term in metallic materials because $\sigma_0 \ll E$ and $n < 0.6$. The validity of Eq. (24) is questionable in stiff solids where $n \rightarrow 1$, as one may not longer assume that $\epsilon_{el} \ll \epsilon_{pl}$ in Eq. (22).

3. Finite element simulations

Finite element simulations were performed for conical, spherical and pyramidal indentation experiments, Fig. 3. Details of the finite element meshes and their density-region hierarchy are given in Mata et al., 2002. The simulations were performed assuming frictionless contact conditions (Mata and Alcalá,

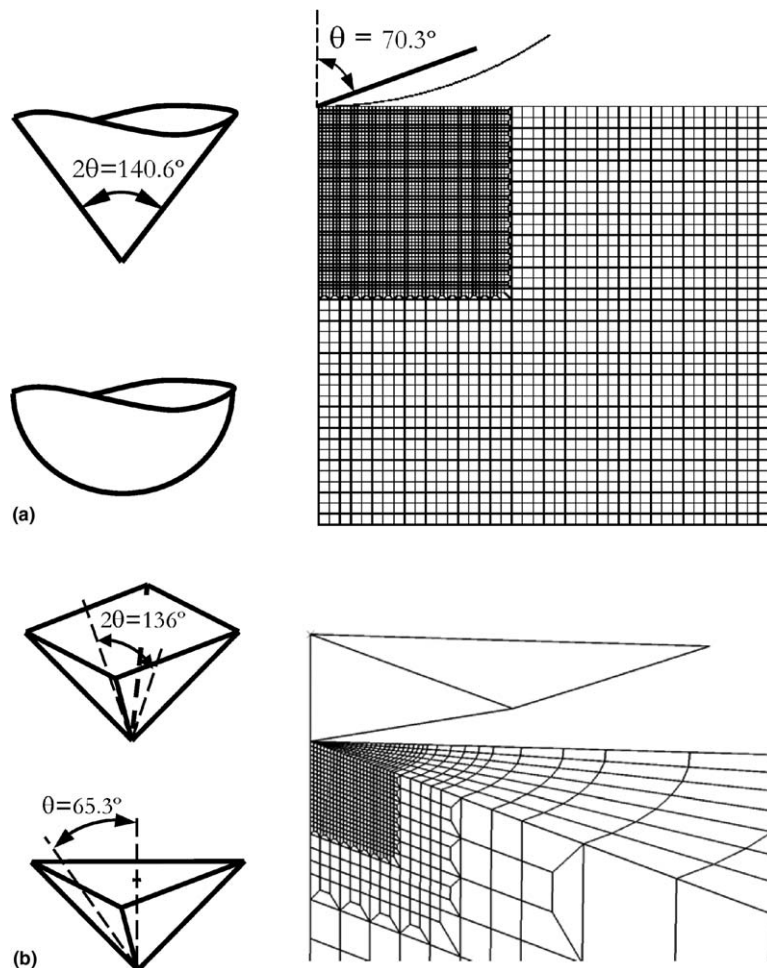


Fig. 3. Finite element meshes used in the (a) axis-symmetric simulations of conical and spherical indentation, and (b) three-dimensional simulations of Vickers indentation (a similar mesh was used for the three-sided Berkovich tip illustrated in the figure).

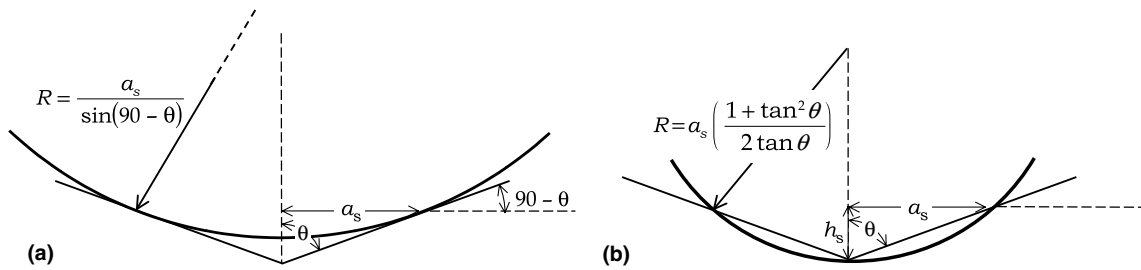


Fig. 4. Schematic of equivalent indentation strains. (a) The sphere is tangent to contact radius a_s , and (b) configuration where the sphere intersects contact radius a_s and penetration depth h_s .

2004). Large strains and rotations were accounted for in all computations, which were also conducted with a full integration scheme. More than 52 elements became in contact with the indenters at maximum penetration depth. Indenter's diameter was scaled so that $a_s/R = 0.75$ at maximum depth (notice that contact radius a_s is defined disregarding development of pileup or sinking-in at the contact periphery, see Fig. 4). The simulations for conical indentation were performed with a tip whose apex angle is 70.3° , for it leads to the same geometrical relation of contact area–penetration depth as the Vickers pyramid. Complementary three-dimensional simulations were performed for the Vickers and the Berkovich pyramidal indenters as described by Giannakopoulos et al. (1994) and Casals and Alcalá (2005).

Table 1

Mechanical properties of the solids used in the simulations of spherical and pyramidal indentation

Indenter			E/σ_r	E (GPa)	σ_{ys}	n
S	V		4000	200	50	0
			1400	70	50	0
		B	700	70	100	0
S	V	B	500	200	400	0
			275	110	400	0
S	V	B	70	70	1000	0
S	V	B	2197	200	50	0.1
		B	1177	200	100	0.1
		B	854	70	50	0.1
		B	458	70	100	0.1
S	V	B	338	200	400	0.1
S		B	148	200	1000	0.1
S	V	B	58	70	1000	0.1
S	V		1207	200	50	0.2
		B	693	200	100	0.2
		B	521	70	50	0.2
		B	229	200	400	0.2
S	V	B	47	70	1000	0.2
S	V	B	364	200	50	0.4
		B	240	200	100	0.4
		B	194	70	50	0.4
		B	105	200	400	0.4
S	V	B	36	70	1000	0.4

Simulations of conical indentation comprised the 48 solids resulting from the combination of $E = 50, 110, 200$ GPa; $\sigma_{ys} = 50, 100, 400, 1000$ MPa; and $n = 0, 0.1, 0.2, 0.4$.

S = sphere, V = Vickers, B = Berkovich.

The indented solids were assumed to obey the J_2 associated-flow plasticity theory. For consistency with the theoretical framework, the uniaxial stress–strain curve was taken to follow Eq. (3). Simulations of conical indentation were performed for 48 solids comprising all combinations of $E = 70, 110$ and 200 GPa; with $\sigma_{ys} = 50, 100, 400$ and 1000 MPa; with $n = 0, 0.1, 0.2, 0.4$. The simulations of spherical indentation, Vickers indentation, and Berkovich indentation were performed for representative solids whose properties are listed in Table 1.

4. The analogy between indentation and the expansion of a cavity

The purpose of this section is to propose a sensible substitution of the parameters in expanding cavity formulations for those in sharp indentation experiments.

We first seek to establish a penetration depth at which the plastic zone induced by a spherical indenter (replacing the cavity) is similar to that existing around a conical tip. Note that the sought-after similarity exclusively concerns the plastic zone and not the stress fields or hardness values. Perhaps the main obstacle in finding such an equivalence is that while the plastic zone in sharp indentation has a self-similar nature, the severity of the deformation field in spherical indentation increases as the ratio of contact radius a_s to indenter's radius R is increased. Thus, as indentation strain a_s/R increases, the contact response evolves from a Hertzian perfectly elastic regime, to an elasto-plastic transition, to the fully plastic regime examined by Tabor. In the absence of length scales, however, the active deformation regime in conical indentation remains constant throughout the entire loading stage by virtue of the self-similar nature of the penetration process. The contact deformation map given by Mata et al. (2002) allows one to predict the active regime in sharp indentation experiments of strain hardening solids with a conical tip of $\theta = 70.3^\circ$. The results were consistent with the fact that the degree of elasto-plasticity increases in solids with a small E or with large σ_{ys} and n .

It is noteworthy that the angle of 136° existing between opposite faces of the Vickers pyramidal indenter was selected based upon a geometrical analogy with the spherical (Brinell) indentation test. In light of this analogy, an equivalent indentation strain a_s/R can be defined so that the spherical tip becomes tangent at the contact boundary of a conical imprint (see Fig. 4(a)). It thus follows that

$$a_s/R = \sin(90^\circ - \theta). \quad (25)$$

Hence, for $\theta = 70.3^\circ$, $a_s/R = 0.342$. Nevertheless, inspection of the finite element simulations reveals that the normalized plastic zone size in the z -axis (z_{ys}/h_s) induced by a spherical indenter at $a_s/R = 0.342$ is larger than that present for the conical indentation (Fig. 5). Overall, the evolution in plastic zone size with a_s/R exhibited in spherical indentation of solids with a large degree of elasto-plasticity is more pronounced than that found in those whose contact response is more plastically dominated (compare Fig. 5(a) with (c)). For a fixed indentation strain, the difference in plastic zone sizes between both tips thus increases as the contact response becomes more elasto-plastic. Notice that while solids indented within the fully plastic contact regime have similar plastic zones for conical and spherical indentation provided $a_s/R > 0.30$, this is not true in elasto-plastic materials where agreement in plastic zone size is only encountered for larger values of a_s/R . Along these lines, circumspective analysis of the finite element simulations reveals that *irrespective of the contact response*, normalized plastic zone sizes z_{ys}/h_s measured at $a_s/R = 0.635$ are the same as those exhibited for conical indentation with $\theta = 70.3^\circ$. As illustrated in Fig. 4(b), this interesting finding enables us to reformulate the aforementioned analogy of the equivalent indentation strain so that the two indenters are enforced to cross each other at contact radius a_s as well as at penetration depth h_s . (Notice that a_s disregards development of pileup or sinking-in at the contact periphery.) Simple geometrical arguments thus yield

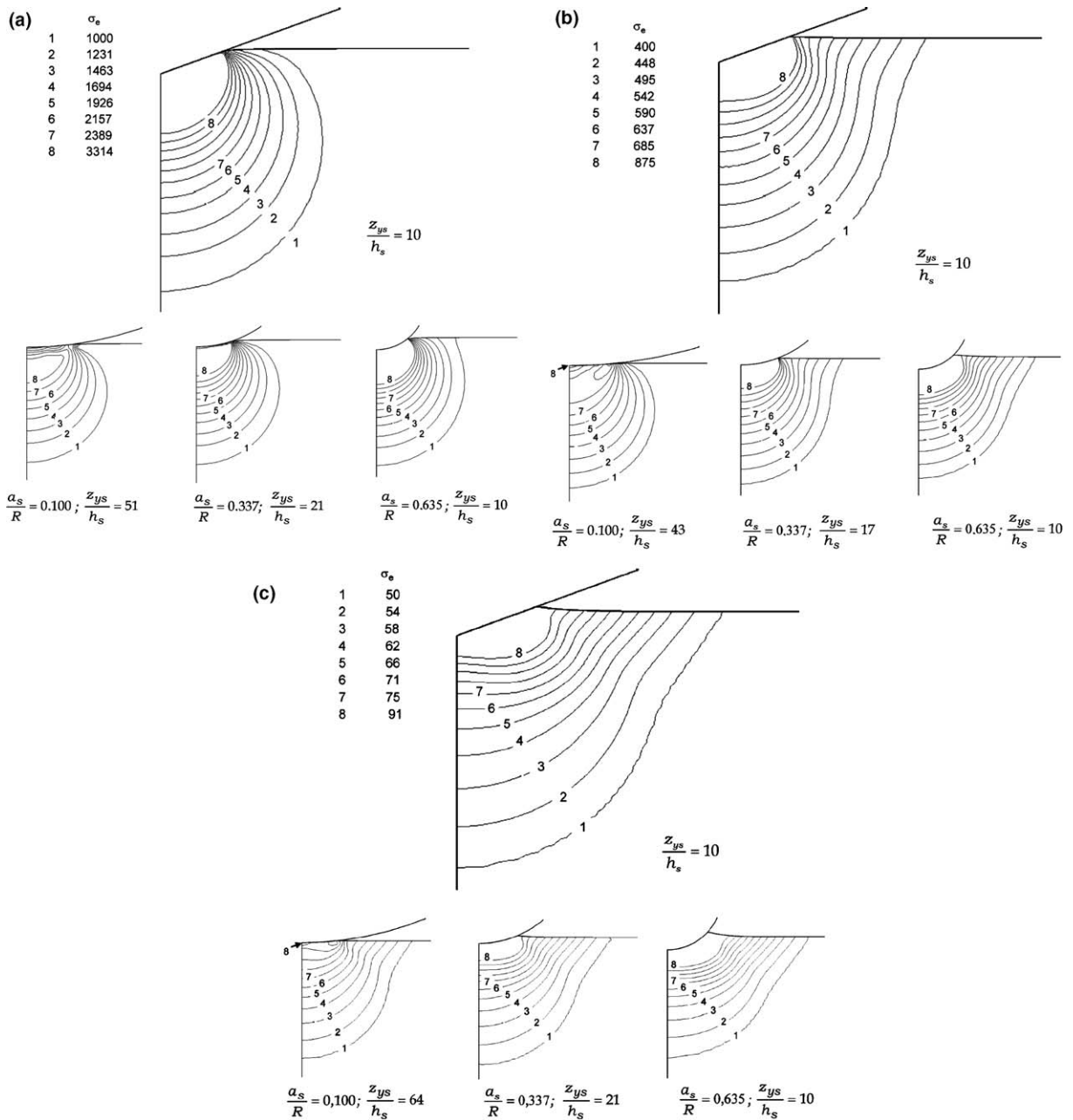


Fig. 5. Comparison of the plastic zone size between conical and spherical indentations at different values of a_s/R for (a) highly elasto-plastic solid ($E = 200$ GPa, $\sigma_{ys} = 1000$ MPa, and $n = 0.4$), (b) a solid with reduced elasto-plastic character ($E = 200$ GPa, $\sigma_{ys} = 400$ MPa, and $n = 0.2$), and (c) a fully plastic solid ($E = 200$ GPa, $\sigma_{ys} = 50$ MPa, and $n = 0.1$). These solids were selected to illustrate the fact that although their values of z_{ys}/h_s are similar, the shape of their plastic zones is strongly dependent on the mechanical properties. It is emphasized that z_{ys}/h_s in any spherical indentation made at $a_s/R = 0.635$ equals that for conical indentation with $\theta = 70.3^\circ$.

$$\frac{a_s}{R} = \frac{2 \tan \theta}{1 + \tan^2 \theta}, \quad (26)$$

so that when $\theta = 70.3^\circ$, a_s/R takes the above value of 0.635. Consequently, cavity radius R in expanding cavity formulations is herein substituted by

$$R = \frac{a_s}{0.635}. \quad (27)$$

Attention is now given to cavity pressure p_{cav} . In the spirit of the analogy between the hydrostatic pressure inflating the cavity and hardness measurements in sharp indentation experiments, we take

$$p_{\text{cav}} = H_L = \frac{H}{f}, \quad (28)$$

where H is the projected hardness, H_L is the Ludwick hardness computed with the curved surface or cavity area of the indentation, and f is a projection factor. For conical indenters $f = 1/\sin\theta$; for the Vickers and the Berkovich indenters $f = 1.079$ and 1.101 , respectively. In addition to assimilating a sharp indenter as the spherical tip replacing the cavity, Eq. (28) underlies a presumed constancy of the pressure distribution because, by definition, hydrostatic pressure p_{cav} takes a constant value throughout the cavity. Thus, it may only be sensible to equate H_L to hydrostatic pressure p_{cav} in solids where the contact pressure distribution is rather constant.

Finally, one has to consider that expanding cavity formulations describe inflation of an infinite space. As described above, comparison between such formulations and indentation experiments is attempted here along the symmetry z -axis, where the influence of the free surface is diminished. Thus, following Fig. 6

$$c = z_{\text{ys}} + R - h_s = z_{\text{ys}} + 1.217a_s, \quad (29)$$

where the equality in the right-hand side holds for the particular case of a conical tip of $\theta = 70.3^\circ$. Notice that although the equivalence in plastic zone size between spherical and conical indentation is predicated upon variable z_{ys}/h_s , the analogy between indentation and the inflation of a cavity is based on formulations which employ ratio c/R . Eqs. (27) and (29) imply that c/R is linearly dependent on z_{ys}/h_s .

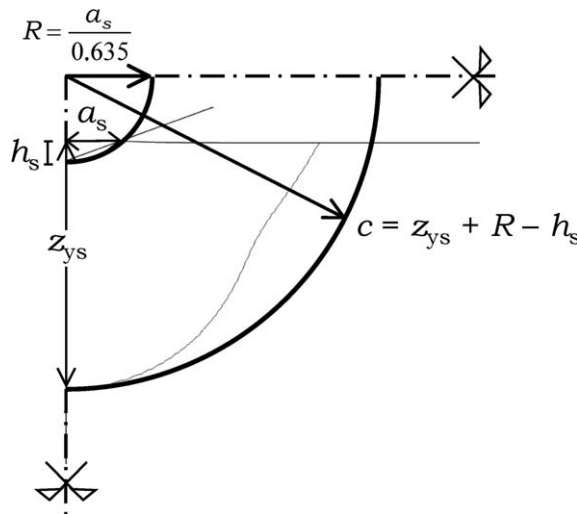


Fig. 6. Schematic of the parametrical analogy between indentation and the expansion of a spherical cavity.

5. Validation of the analogy

5.1. Elastic–perfectly plastic solids

In the following discussion, the proposed parametrical analogy between indentation experiments and the inflation of the cavity is examined. Essentially, we seek to establish the applicability of Eqs. (7) and (8) to the analysis of indentation experiments in perfectly plastic solids ($n = 0$). This is performed by recourse to the finite element simulations of conical indentation, which provide contact radius a_s , plastic zone size z_{ys} , and hardness H for a given solid indented to a fixed penetration depth h_s .

Substitution of Eqs. (27)–(29) into Eqs. (7) and (8) yields

$$\frac{H}{\sigma_{ys}} = f \cdot \left[\frac{2}{3} + 2 \ln \left(\frac{z_{ys} + 1.217a_s}{a_s/0.635} \right) \right], \quad (30)$$

and

$$\frac{c}{R} = \frac{z_{ys} + 1.217a_s}{a_s/0.635} = \left(\frac{2E}{3\sigma_{ys}} \right)^{1/3}. \quad (31)$$

Since the finite element simulations for $n = 0$ show that $H/\sigma_{ys} = 2.57$ irrespectively of the mechanical properties of the solid (Mata and Alcalá, 2003), substitution of this equality into Eq. (30) suggests saturation of the logarithmic term and, thus, of relative plastic zone size c/R (see Figs. 7 and 8). The trends predicted through Eq. (30) are in very good accord with the finite element simulations. Interestingly, however, Eq. (31) strongly overestimates c/R and does not capture the feature of its saturation, see Fig. 9 for $\sigma_r = \sigma_{ys}$ ($n = 0$). It is noted that while c/R is assimilated as $\frac{(z_{ys} + 1.217a_s)}{a_s/0.635}$ in present parametrical analogy, overestimation of relative plastic zone size is also found when taking $c/R = c/a_s$ as in Johnson's indentation model, Fig. 9.

The above-mentioned discrepancy between Eqs. (30) and (31) seems to lie in the fact that integration limits $c_0 = R_0 = 0$ (Section 2.1) are not physically acceptable solutions. This is because the elastic–plastic boundary develops following some early state, where cavity inflation is purely elastic. Since c appears after

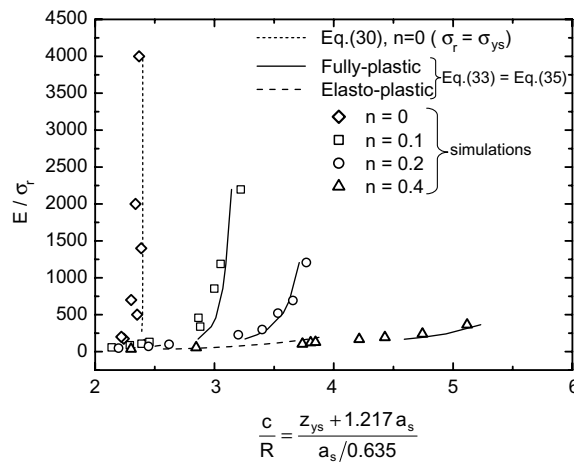


Fig. 7. Correlation between E/σ_r and relative plastic zone size c/R in conical indentation of solids with different values of n . Short dashes correspond to the expanding cavity solution for elastic–perfectly plastic solids in Eq. (30), which is equated to $H/\sigma_{ys} = 2.57$. Solid lines correspond to the fully plastic solution for strain-hardening solids, found by equating Eqs. (33)–(35). Large dashes concern the elasto-plastic solution where in the above equality, $\Theta(n)$ is replaced by $\Theta_{ep}(n)$.

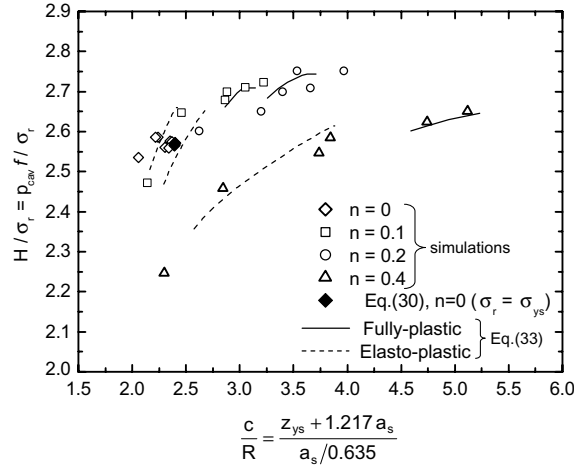


Fig. 8. Comparison between the expanding cavity equations and the simulations of conical indentation. Solid line represents the fully plastic response given through Eq. (33). Dashed line corresponds to the elasto-plastic solution of Eq. (33), where $\theta_{ep}(n)$ is employed replacing $\theta(n)$.

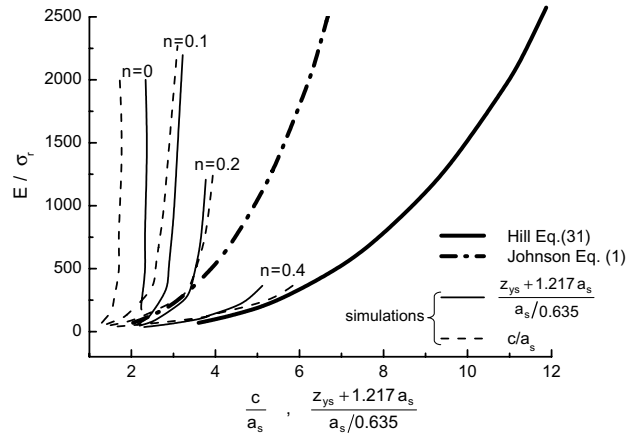


Fig. 9. Comparison between relative plastic zone size from Hill's expanding cavity formulation for $n = 0$, Johnson's indentation model for the relative indentation plastic zone size c/a_s , and current finite element simulations. Simulations where relative plastic zone sizes are defined as c/a_s and as $\frac{(z_{ys} + 1.217 a_s)}{a_s / 0.635}$ are compared against Johnson's indentation model and Hill's formulation, respectively. For $n > 0$, σ_{ys} is replaced by σ_r following Johnson's considerations in extending Hill's formulation to strain hardening solids. In this figure, σ_r is taken at $\epsilon = 0.072$ as in Johnson's work (visually similar results are obtained when σ_r is defined at $\epsilon = 0.1$ as in Mata et al., 2002).

such elastic cavity growth from $R = 0$, the initial state $c_0 = R_0 = 0$ is exclusively valid in solids whose $\sigma_{ys} = 0$. (As it is only in such solids where plastic flow commences immediately upon inflation of the cavity.) Consequently, it is for $\sigma_{ys} = 0$ that the expansion of the cavity has a self-similar nature in the sense that the instantaneous plastic zone size can be obtained from any previous state, *including* $R_0 = 0$. It is noted that the presumption of similarity was not made in deriving Eq. (7), from where Eq. (30) originated. Along these lines, deviation between Johnson's model (Eq. (1)) and the finite element simulations is inherent to the lack of similarity in cavity inflation from $R_0 = 0$.

It is remarked that in the analogy between indentation and the expansion of the cavity proposed by Johnson, the cavity was taken to encompass the indenter and some of the material located directly underneath the tip. In the present work, however, the cavity has the perhaps more simple interpretation of being the indenter itself, which applies pressure to the solid. One may argue that the present analogy is an arbitrary one as it would have also been possible to take any alternative definition of R and c in Eq. (7) while changing constants $2/3$ and 2 to capture the trends from the finite element simulations. In addition to strictly preserving the functional forms of expanding cavity formulations, current parametrical analogy has the advantage of holding true when the analysis of indentation experiments in *strain hardening solids* comes into its own, see Section 5.2.

It remains to be mentioned that in Johnson's indentation model for elastic–perfectly plastic solids, Eq. (1) is substituted into Eq. (7) to obtain the following relation between H/σ_{ys} and E/σ_{ys} :

$$\frac{H}{\sigma_{ys}} = \frac{4}{3} + \frac{2}{3} \ln \left(\frac{1}{3 \tan \theta} \frac{E}{\sigma_{ys}} \right). \quad (32)$$

To derive Eq. (32) Johnson thus takes $c/R = c/a_s$, where imprint size a_s is assumed to be equal to the hydrostatic core radius; and p_{cav} as the pressure exerted by the core upon the surrounding media ($p_{cav} = H - 2\sigma_{ys}/3$, Johnson, 1985). Eq. (32) is regarded to apply within the elasto-plastic transition as it matches experimental results within reasonable accuracy; i.e., ratio H/σ_{ys} is found to increase gradually with $E/(\sigma_{ys} \tan \theta)$, where $1/\tan \theta = \tan \beta$ in Johnson's work. The value of H/σ_{ys} is then enforced to saturate at about 3 for $E/(\sigma_{ys} \tan \theta) \approx 30$, in accordance with slip-line analysis for the fully plastic regime (Hill, 1950; Johnson, 1985). It is noteworthy, however, that since Eq. (1) is predicated upon the same similarity arguments as Eq. (8), the resulting Eq. (32) shall only apply to contacts where the role of elasticity is negligible (i.e., for $\sigma_{ys} = 0$). This is a somewhat contradictory observation because it is precisely for $\sigma_{ys} = 0$ where the fully plastic regime rules contact and Eq. (32) ceases to match experimental results.

5.2. Elastic–strain hardening solids

We now direct attention to the applicability of expanding cavity formulations to indentation experiments of strain-hardening solids ($n > 0$). A simple proposal to perform this type of analysis is to replace σ_{ys} by σ_r in Eq. (1) (Johnson, 1970). Fig. 9 shows that this approach is inaccurate because, as indicated in Section 5.1, Eq. (1) may only apply to materials with vanishing σ_{ys} . Moreover, substitution of σ_{ys} by σ_r is insufficient to capture for the dependency of the normalized plastic zone size upon strain hardening parameter n , Fig. 9.

Overall, the finite element simulations show that for a fixed E/σ_r , the plastic zone spreads outwards with increasing n , Fig. 7. This finding is consistent with the results of increasing plastic zone size with increasing n in Fig. 10. It is noteworthy from Fig. 10 that when $n \ll 1$, the plastic zone size differs considerably to that obtained by applying the von Mises yield condition to the elastic solution ($n = 1$).

Following the present parametrical analogy (Eqs. (27)–(29)), Eq. (17) is rewritten as

$$\frac{H}{\sigma_r} = f \cdot \left[\frac{2}{3} \left(\frac{\epsilon_{ys}}{0.1} \right)^n + \Theta(n) + M(n) \left(\frac{z_{ys} + 1.217a_s}{a_s/0.635} \right)^{P(n)} \right]. \quad (33)$$

Since the influence of elastic strains was neglected in deriving Eq. (17), Eq. (33) is in principle limited to solids whose contact response is plastically dominated. Notice that elasticity is incorporated through the third term in the right-hand side of Eq. (24), which is missing in Eqs. (17) and (33). To assess the role of elasticity, the finite element simulations allow us to find function $\Theta_{ep}(n)$ which, when replaced by $\Theta(n)$, ensures applicability of Eq. (33) to elastoplastic contact responses ($E/\sigma_r \leq 110$ (Mata et al., 2002)):

$$\Theta_{ep} = 3.3556 + \frac{0.5122}{n}. \quad (34)$$

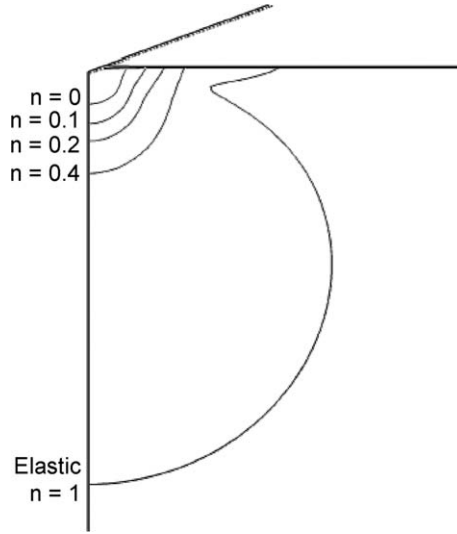


Fig. 10. Influence of strain-hardening parameter n on the plastic zone size. The results are for $E = 200$ GPa and $\sigma_{ys} = 50$ MPa.

Function $\Theta_{ep}(n)$ is an approximative function in the sense that it neglects dependency on σ_0 and E of the third term in Eq. (24).

Fig. 8 shows that Eq. (33) is an accurate formulation in solids deforming within the fully plastic regime (where original function $\Theta(n)$ is used), as well as in elasto-plastic ones (where function $\Theta_{ep}(n)$ is employed). A general relationship between the uniaxial stress–strain curve and the size of the plastic zone is then found equating Eq. (33) to the hardness relation given by Mata and Alcalá (2003):

$$\frac{H}{\sigma_r} = -0.0023 \left[\ln \left(\frac{E}{\sigma_r} \right) \right]^4 + 0.0647 \left[\ln \left(\frac{E}{\sigma_r} \right) \right]^3 - 0.6817 \left[\ln \left(\frac{E}{\sigma_r} \right) \right]^2 + 3.1968 \left[\ln \left(\frac{E}{\sigma_r} \right) \right] - 2.9261. \quad (35)$$

Fig. 7 reveals that the resulting equality is in accordance to the finite element simulations for all fully plastic and elasto-plastic solids.

6. Pyramidal indentation and surface estimates of plastic zone size

The objective of this section is to illustrate the use of present indentation model in the assessment of the plastic zone size *along the indented surface*, as well as to extend the current analysis to Vickers and Berkovich indentation.

First, it is relevant to consider issues of indenter's tip three-dimensionality in present formulations. Following Section 4, the finite element simulations showed that normalized plastic zone size z_{ys}/h_s (or, equivalently, c/R) is the same for conical and spherical indentation provided indentation strain a_s/R is set at 0.635. Present simulations also suggest that this finding holds for pyramidal indenters when a_s is measured at an angle of 25° from the corners of Vickers and Berkovich imprints (see Fig. 11(a) and (b), and Fig. 12).

Another important aspect in the experimental application of present framework concerns the fact that further plastic flow is found to be promoted upon unloading from peak indentation load, see Fig. 13(a) and (b). In this regard, the simulations for Vickers, Berkovich and conical indentation show that the stress field

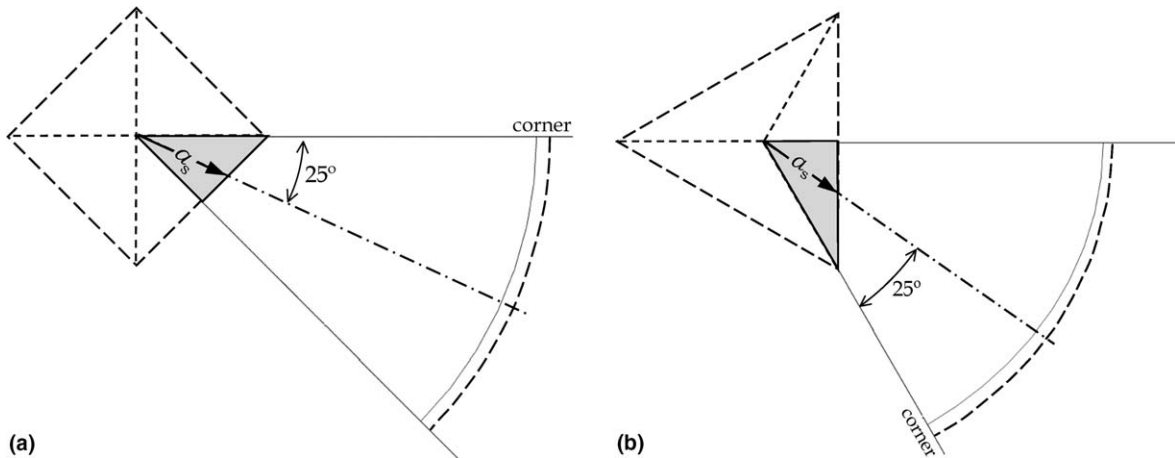


Fig. 11. Illustration of equivalent contact radius a_s for (a) Vickers indentation, and (b) Berkovich indentation. Solid and dashed lines represent the plastic zone at peak load and upon complete unloading, respectively. The simulations are for $E = 70$ GPa, $\sigma_{ys} = 50$ MPa, and $n = 0.2$.

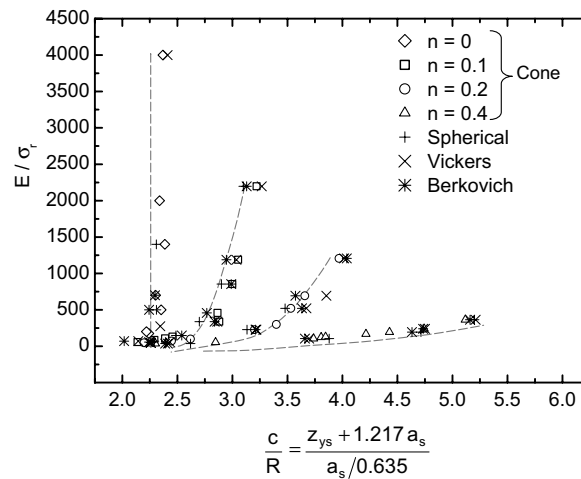


Fig. 12. Similarity in plastic zone sizes for conical, spherical ($a_s/R = 0.635$), and pyramidal indenters. In the latter, a_s is defined following Fig. 11.

outside the plastic zone decreases upon unloading except for the solid lying at vicinity of the free surface, where the equivalent von Mises stress increases facilitating plastic flow (see Fig. 13(a)). Interestingly, the growth of the plastic zone at the surface depends on the contact response of the solid. Overall, this phenomenon is enhanced in solids exhibiting an elasto-plastic transition rather than in those where the fully plastic regime rules the contact response (compare Fig. 13(a) with (b)). It is also noted that upon load removal, the plastic zone at the surface in elasto-plastic contacts bends outwards from the imprint, resembling the shape present in fully plastic indentations. These findings are not due to reverse plasticity as plastic flow upon unloading is not induced by residual compressive stresses but, instead, by an increase in the magnitude of the tensile stresses close to the surface. Thus, consideration of kinematic hardening effects in the plasticity model shall not alter present results.

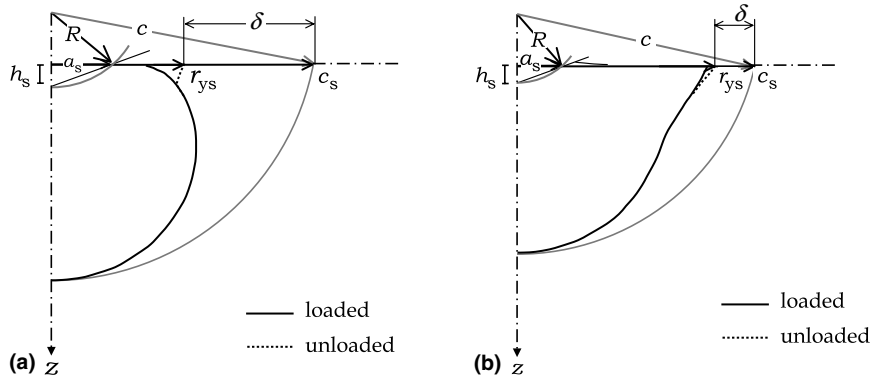


Fig. 13. Plastic zone size for (a) an elasto-plastic solid with $E = 200$ GPa, $\sigma_{ys} = 1000$ MPa, and $n = 0.4$; and (b) a fully plastic material with $E = 200$ GPa, $\sigma_{ys} = 50$ MPa, and $n = 0.1$. Notice the growth of the plastic zone (short dashes) close to the surface and its constancy in the z -axis.

An interesting feature from the simulations of Vickers, Berkovich and conical indentation is that the plastic zone is not continuous in solids with a strong elasto-plastic character. As shown in Fig. 14, an unplastified surface region remains embedded within the plastic zone. Upon unloading, plastic flow occurs gradually at the periphery of such region, decreasing its size.

According to the present simulations, the value of δ/c_s in terms of E/σ_r is found to be well fitted through (see Figs. 13 and 15)

$$\frac{\delta}{c_s} = \left(-19.754 + 1.00974 \left(\frac{E}{\sigma_r} \right) \right)^{-0.23256} \quad (36)$$

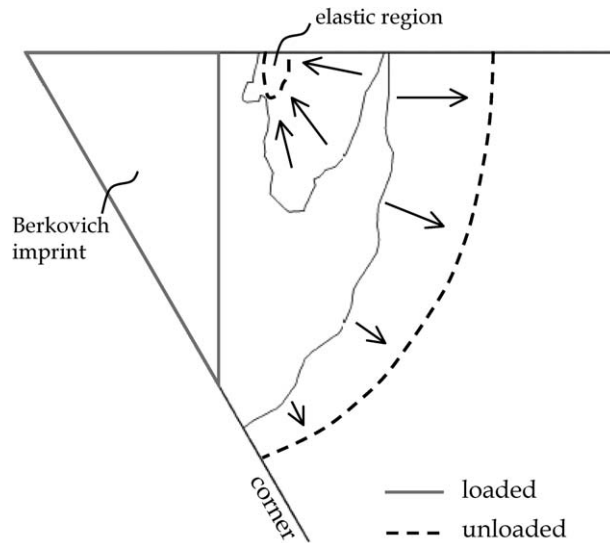


Fig. 14. Comparison between the plastic zone for Berkovich indentation at maximum load (solid line) and upon complete unloading (dashed line) for a highly elasto-plastic solid ($E = 70$ GPa, $\sigma_{ys} = 850$ MPa, and $n = 0.2$). Arrows indicate direction of plastic flow during unloading. Notice that the elastic region embedded within the plastic zone decreases its size upon load removal.

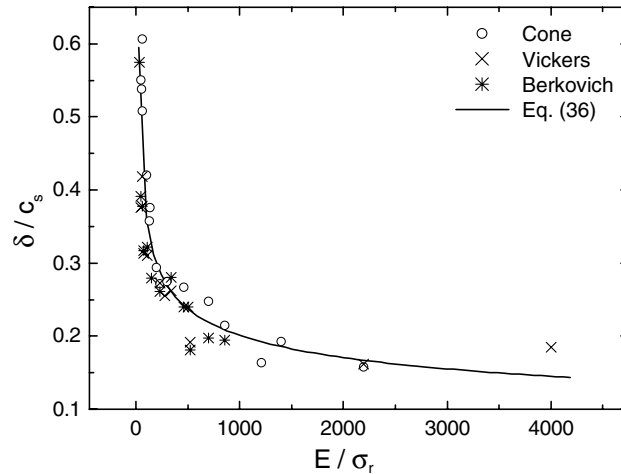


Fig. 15. Correlation between δ/c_s and E/σ_r for the conical and the pyramidal indenters (see Fig. 13 which defines δ and c_s).

for Vickers, Berkovich and conical indentations. The schematic in Fig. 13 also indicates that

$$\frac{c_s}{R} = \sqrt{\left(\frac{c}{R}\right)^2 - 0.5868} \quad (37)$$

for the conical tip with $\theta = 70.3^\circ$ as well as for the Vickers and the Berkovich indenters, where a_s is defined as in Fig. 11. Therefore, to estimate the plastic zone size r_{ys} at the surface in a material whose uniaxial mechanical properties are known a priori, one has to measure hardness H and imprint size a_s . Then, calculate $c/R = \frac{(z_{ys} + 1.217a_s)}{a_s/0.635}$ from Eq. (30) in solids where $n = 0$, or from Eq. (33) when $n > 0$. Find R through Eq. (27) and compute c_s from Eq. (37). Finally, obtain δ through Eq. (36), so that

$$r_{ys} = c_s - \delta. \quad (38)$$

7. Summary

In this investigation, a new indentation model based on the analogy of the expansion of a spherical cavity has been proposed. The derived equations allow one to perform accurate assessments of plastic zone size in conical and pyramidal indentation experiments.

The following are the central findings of the work.

1. Derivation of closed-form solutions for the plastic zone size cannot be strictly based on the assumption of a vanishingly small plastic zone at the commencement of cavity inflation. That is, one cannot take $R_0 = c_0 = 0$ because the early elastic response during cavity expansion breaks-out the self-similar nature of the process. The presently derived solutions that were not predicated upon such similarity arguments allowed us to extend prior analysis for perfectly plastic solids to strain hardening media ($n \neq 0$). Overall, it is found that strain hardening has a profound effect on the inflation of the cavity and on the plastic zone size. Such strain hardening effects cannot be captured through a simple substitution of yield strength σ_{ys} with representative stress σ_r in perfectly plastic formulations.
2. The present analysis in conjunction with finite element simulations allowed us to develop an accurate analogy between the variables in expanding cavity formulations and those ruling indentation

experiments. This parametrical analogy is based on the concept of an equivalent spherical indenter which, regardless of the mechanical properties of the material, induces the same plastic zone size in the z -axis as a conical tip. A distinctive feature of present parametrical analogy is that the explicit closed-form solutions derived for the expansion of the cavity directly apply to the analysis of indentation experiments of both perfectly plastic and strain hardening solids.

3. Three-dimensional finite element simulations enable extension of the present framework to Vickers and Berkovich pyramidal indentation. It is found that the shape of the plastic zones induced by a conical indenter of $\theta = 70.3^\circ$ is maintained at an angle of 25° from the corners of Vickers and Berkovich imprints. Interestingly, considerable plastic flow may occur at the surface upon complete load removal in solids with a highly elasto-plastic character. Simple guidelines are provided in the paper for the assessment of the plastic zone remnant along the indented surface in pyramidal and conical indentation experiments.

Acknowledgments

M.M. and O.C. wish to thank doctoral scholarship programs from the Spanish Ministry of Education and Science (MEC) and Generalitat de Catalunya. This work was partly funded by MEC and CICYT through Grant No. MAT 2002-00368 and PETRI Grant No. 95-0763.OP.01.

References

- Atkins, A., Tabor, D., 1965. Plastic indentation in metals with cones. *J. Mech. Phys. Solids* 13, 149.
- Bignoni, D., Ludiero, F., 1989. The quasi-static finite cavity expansion in a non-standard elasto-plastic medium. *Int. J. Mech. Sci.* 31, 825–837.
- Bishop, R.F., Hill, R., Mott, F.R.S., 1945. The theory of indentation and hardness tests. *Proc. Phys. Soc.* 57, 147–159.
- Casals, O., Alcalá, J., 2005. The duality in mechanical property extractions from Vickers and Berkovich instrumented indentation experiments. *Acta Mater.* 53, 3545–3561.
- Chadwick, P., 1959. The quasi-static expansion of a spherical cavity in metals and ideal soils. *Quart. J. Mech. Appl. Math.* 12, 52–71.
- Chiang, S.S., Marshall, D.B., Evans, A.G., 1982. The response of solids to elastic/plastic indentation. I. Stresses and residual stresses. *J. Appl. Phys.* 53, 298–311.
- Chiu, Y.L., Ngan, A.H.W., 2002. A TEM investigation on plastic zones in Ni3Al(Cr,B) single crystals. *Acta Mater.* 50, 2677–2691.
- Dao, M., Chollacoop, N., Van Vliet, K.J., Venkatesh, T.A., Suresh, S., 2001. Computational modelling of the forward and reverse problems in instrumented indentation. *Acta Mater.* 49, 3899–3918.
- Durban, D., Baruch, M., 1976. On the problem of a spherical cavity in an infinite elasto-plastic medium. *J. Appl. Mech.* December, 633–638.
- Elmustafa, A.A., Stone, D.S., 2002. Indentation size effect in polycrystalline F.C.C. metals. *Acta Mater.* 50, 3641–3650.
- Elmustafa, A.A., Eastman, J.A., Rittner, M.N., Weertman, J.R., Stone, D.S., 2000. Indentation size effect: large grained aluminum versus nanocrystalline aluminum-zirconium alloys. *Scr. Mater.* 43, 951–955.
- Giannakopoulos, A.E., Larsson, P.-L., Vestergaard, R., 1994. Analysis of Vickers indentation. *Int. J. Solids Struct.* 31, 2679–2708.
- Hill, R., 1950. *The Mathematical Theory of Plasticity*. Oxford University Press, New York.
- Huang, Y., Xue, Z., Gao, H., Nix, W.D., Xia, Z.C., 2000. A study of microindentation hardness tests by mechanism-based strain gradient plasticity. *J. Mater. Res.* 15, 1786–1796.
- Johnson, K.L., 1970. The correlation of indentation experiments. *J. Mech. Phys. Solids* 18, 115–126.
- Johnson, K.L., 1985. *Contact Mechanics*. Cambridge University Press, Cambridge, UK.
- Kramer, D., Huang, H., Kriese, M., Robach, J., Nelson, J., Wright, A., Bahr, D., Gerberich, W.W., 1999. Yield strength predictions from the plastic zone around nanocontacts. *Acta Mater.* 47, 333–343.
- Larsson, P.-L., 2001. Investigation of sharp contact at rigid-plastic conditions. *Int. J. Mech. Sci.* 43, 895–920.
- Li, H., Bradt, R.C., 1993. The microhardness indentation load/size effect in rutile and cassiterite single crystals. *J. Mater. Sci.* 28, 917–926.
- Lubliner, J., 1990. *Plasticity Theory*. Macmillan Publishing Company, USA.
- Mata, M., Alcalá, J., 2003. Mechanical property evaluation through indentation experiments in elasto-plastic and fully plastic contact regimes. *J. Mater. Res.* 18, 1705–1709.

- Mata, M., Alcalá, J., 2004. The role of friction in sharp indentation. *J. Mech. Phys. Solids* 52, 145–165.
- Mata, M., Anglada, M., Alcalá, J., 2002. Contact deformation regimes around sharp indentations and the concept of the characteristic strain. *J. Mater. Res.* 17, 964–976.
- Puech, P., Pinel, S., Jasinevicius, R.G., Pizani, P.S., 2000. Mapping the three-dimensional strain field around a microindentation on silicon using polishing and Raman spectroscopy. *J. Appl. Phys.* 88, 4582–4585.
- Tabor, D., 1951. *Hardness of Metals*. Clarendon Press, United Kingdom.
- Woodcock, C.L., Bahr, D.F., 2000. Plastic zone evolution around small scale indentations. *Scr. Mater.* 43, 783–788.
- Xu, Z.-H., Rowcliffe, D., 2002. Method to determine the plastic properties of bulk materials by nanoindentation. *Philos. Mag. A* 82, 1893–1902.
- Yoshioka, M., 1994. Plastically deformed region around indentations on Si single crystal. *J. Appl. Phys.* 76, 7790–7796.